FEBS Letters

FEBS PRESS science publishing by scientists

A real-time cell-binding assay reveals dynamic features of STxB–Gb3 cointernalization and STxB-mediated cargo delivery into cancer cells

João Crispim Encarnação[1,2], Valeria Napolitano[3,4], Giulia Opassi[5], U. Helena Danielson[5], Grzegorz Dubin[3], Grzegorz M. Popowicz[6,7], Hélène Munier-Lehmann[8], Jos Buijs[1,2], Karl Andersson[1,2] and Hanna Björkelund[1]

1 Ridgeview Instruments AB, Uppsala, Sweden
2 Department of Immunology, Pathology and Genetics, Rudbeck Laboratory, Uppsala University, Uppsala, Sweden
3 Malopolska Centre of Biotechnology, Jagiellonian University, Krakow, Poland
4 Faculty of Biochemistry, Biophysics and Biotechnology, Jagiellonian University, Krakow, Poland
5 Department of Chemistry-BMC, Uppsala University, Uppsala, Sweden
6 Institute of Structural Biology, Helmholtz Zentrum München, Neuherberg, Germany
7 Center for Integrated Protein Science Munich at Chair of Biomolecular NMR, Department Chemie, Technische Universität München, Garching, Germany
8 Unité de Chimie et Biocatalyse, Département de Biologie Structurale et Chimie, Institut Pasteur, CNRS UMR3523, Paris, France

Correspondence
J. Crispim Encarnação, Ridgeview Instruments AB, Dag Hammarskjölds väg 36A, Science Park, Uppsala 75237, Sweden
Tel: +46 73 073 54 83
E-mail: joao.encarnacao@ridgeview.eu

João Crispim Encarnação and Valeria Napolitano have contributed equally to this work

(Received 23 March 2020, revised 16 May 2020, accepted 19 May 2020, available online 23 June 2020)

doi:10.1002/1873-3468.13847

Edited by Lukas Alfons Huber

The interaction between the Shiga toxin B-subunit (STxB) and its globotriaosylceramide receptor (Gb3) has a high potential for being exploited for targeted cancer therapy. The primary goal of this study was to evaluate the capacity of STxB to carry small molecules and proteins as cargo into cells. For this purpose, an assay was designed to provide real-time information about the StxB–Gb3 interaction as well as the dynamics and mechanism of the internalization process. The assay revealed the ability to distinguish the process of binding to the cell surface from internalization and presented the importance of receptor and STxB clustering for internalization. The overall setup demonstrated that the binding mechanism is complex, and the concept of affinity is difficult to apply. Hence, time-resolved methods, providing detailed information about the interaction of STxB with cells, are critical for the optimization of intracellular delivery.

Keywords: binding kinetics; cancer; cell surface receptor; real-time cell-binding assays; receptor internalization; Shiga toxin

One of the major challenges of cancer therapy is selectivity. Compounds that target cancer cells with high specificity minimize the risk of side effects in healthy tissue, thus potentially improving the quality of life for patients [1]. Discovering vectors that bind to cell surface molecules that are specific for, or overproduced by, cancer cells enables the design of therapies that target cancer with higher specificity [2]. Targeting strategies where a chemotherapeutic agent is conjugated to a carrier, such as a monoclonal antibody, have been described and are being further explored for improving drug efficiency. This strategy of combining cytotoxic drugs with antibodies, termed antibody-drug conjugates, has already resulted in approved medications, for example, brentuximab, vedotin, and adotrastuzumab emtansine [3]. However, resistance to

Abbreviations
eGFP, enhanced green fluorescent protein; FITC, fluorescein isothiocyanate; Gb3, globotriaosylceramide; RT-CBA, real-time cell-binding assays; STxB, Shiga toxin subunit B.

FEBS Letters **594** (2020) 2406–2420 © 2020 The Authors. *FEBS Letters* published by John Wiley & Sons Ltd on behalf of Federation of European Biochemical Societies
This is an open access article under the terms of the Creative Commons Attribution License, which permits use, distribution and reproduction in any medium, provided the original work is properly cited.

these drugs has been reported, caused by mechanisms such as impaired lysosomal function or antigen-related resistance [4].

To evade resistance, modified treatment strategies for delivery of conjugates into cells are desired. One alternative is presented by Shiga toxin. This toxin is produced by intestinal pathogenic bacteria such as *Shigella dysenteriae* and shigatoxigenic serotypes of *Escherichia coli* (STEC). It is composed of two subunits (A and B) with distinct roles. The nontoxic subunit B is a pentameric protein that binds the toxic subunit A and is then instrumental in a mechanism that internalizes the complex into cells upon which subunit A is released. Since Shiga toxin is an intestinal virulence factor with high stability in different physiological environments, the toxin has received considerable attention [5]. The reason why Shiga toxin can internalize in cells is because the B-subunit (STxB) specifically binds to its natural globotriaosylceramide receptor (Gb3, also known as CD77 and ceramide trihexoside) on mammalian cells [6]. Interestingly, Gb3 is not a protein, but a globoside consisting of galactose linked to lactosylceramide. Three trisaccharide molecules are bound to each B-subunit monomer, orienting the toxin on the surface and the multivalent interactions contribute to a high functional affinity or avidity. Moreover, this initiates a membrane reorganization, and induces curvature and toxin clustering, the first step in the formation of tubular endocytic pits [7]. Thus, once STxB binds to Gb3 at the cell surface, it is rapidly internalized by endocytosis, reaching the early and recycling endosomes [8]. STxB can thereafter escape the late endocytic pathway through an intracellular trafficking termed the retrograde route, thus avoiding the extreme environment of lysosomes [9]. The internalization mechanism of STxB has been extensively studied, and it has been observed that STxB, once bound to the lipid bilayer, has the capacity to form membrane invaginations by glycolipid receptor clustering. It has also been reported that STxB binds to Gb3 by both the dependent clathrin machinery and independent clathrin machinery [10].

Some human cancers, such as lymphomas and colorectal carcinomas, have high levels of Gb3 exposed on their outer cell surface. Cancer cells have up to 10^8 binding sites for STxB [11], whereas there are typically at most 10^6–10^7 binding sites for antibodies per target cell, as, for example, shown for the EGFR-binding antibody cetuximab [12]. STxB may therefore be an effective carrier for delivering small peptides or molecules into cancer cells, and STxB conjugated with different drugs, such as auristatin derivatives and SN-38, has consequently been explored [11,13]. Different strategies for conjugating drugs with the STxB subunit have been applied, for example, using cysteine coupling or linkers that allow drug-release upon reaching a reducing environment [14].

At the molecular level, different aspects of the interaction between STxB and Gb3 have been investigated. It includes studying the interaction between the molecules by SPR-biosensor assays [15,16], assessing the ability of STxB to form membrane invagination by using giant unilamellar vesicles or investigating intracellular events through microscopy [17]. However, defining the interaction characteristics by biophysical methods requires artificial approximations in nonphysiological conditions: in particular, does not account for the importance of specific moieties in the glycolipids and the toxin for the interactions (i.e., not employing a lipid bilayer system). Such simplified systems may not adequately reflect the actual events occurring on the cell membrane or the stimuli of biological processes [18]. Experiments have also been performed under conditions that mimic cell membrane environments, resulting in different apparent affinities ranging from high (521 nM) to low (8 nM) nanomolar range [16,17]. For interactions on cells, it has been observed that the apparent affinity ranges between 4.7 and 80 nM, depending on the cell type [19,20]. The complexity of the cell membrane and the different species of the Gb3 receptor on different cell lines imply that it is a system that is difficult to mimic with assays that employ receptors outside their cellular environment.

This complexity might partly be caused by the clustering of the plasma membrane receptors upon ligand binding. For example, it has been described that unstimulated lipid raft domains are usually small (2–10 nm), extremely dynamic and ephemeral (1 ns–1 s). In contrast, upon external stimuli, raft-associated receptors cluster together to form stable, larger domains in the size range of 10–20 nm that possess a longer lifetime [21]. Glycolipid receptor clustering upon STxB binding to a lipid bilayer is an example of this phenomenon. The reason may be the interaction between STxB and up to 15 Gb3 molecules, leading to a contraction of lipids underneath the protein, and a local thickening of the membrane. Once STxB binds to the outer membrane leaflet, clustered ligand–receptor mass exerts a local stress on the toxin-binding site which translates into negative membrane curvature. This, in turn, leads to an increased surface area that facilitates additional ligand binding. As a result of this local compaction of lipids, more ligand molecules bind and boost the membrane deformation, thus leading to tubule formation once a critical concentration of ligand–receptor clusters is achieved [22].

In this study, our primary goal was to evaluate the capacity of STxB to carry big and small cargo molecules into cells. By conjugating STxB with a green fluorescent protein (eGFP) or with fluorescein (FITC), the binding and delivery capacity as function of temperature, time, and concentration could be estimated for the two types of cargo. To obtain detailed information on the apparent kinetics and apparent affinity of the STxB–Gb3 interaction, as well as the internalization processes, we employed a real-time cell-binding assay (RT-CBA) [23]. Discrepancies between the STxB binding and internalization rates obtained with RT-CBA and reported results from end point measurements [24] were observed. RT-CBA was therefore used to further explore the interaction and internalization mechanisms of the STxB constructs. Additionally, proximity assays between STxB fluorescent and quenched labeled forms were performed to evaluate the impact of time on the STxB binding, proximity, and compaction to Gb3 receptors.

Materials and methods

Cloning, proteins expression, and purification

A pET46 expression plasmid containing the gene encoding full-length subunit B of Shiga toxin (STxB) type I with an N-terminal hexahistidine tag was provided by Helmholtz Zentrum, Munich. A second construct (STxB–eGFP) was made by using the STxB containing plasmid as a template for PCR amplification of the gene. Thereafter, the eGFP gene was fused to the C-terminal of STxB through a GSGS linker *via* PCR. The amplified product was later inserted into a pETSumo expression vector (HMGU library) between BsaI and NotI restriction sites.

STxB and STxB–eGFP with His-tags were expressed in *E. coli* BL21 (DE3) cells grown in LB medium supplemented with 100 $\mu g \cdot mL^{-1}$ ampicillin (STxB) or 50 $\mu g \cdot mL^{-1}$ kanamycin (STxB–eGFP). The cells were grown at 37 °C until the optical density (OD_{600}) of the culture reached 0.7. The temperature was then lowered to 20 °C, and isopropyl b-D-1-thiogalactopyranoside was added to a final concentration of 1 mM. The cells were allowed to grow overnight where after they were harvested by centrifugation for 15 min at 6000 ***g***, resuspended in lysis buffer (PBS pH 8.0; Medicago AB, Uppsala, Sweden) supplemented with protease inhibitors—(cOmplete™ EDTA-free; Roche, Basel, Switzerland), 10 $\mu g \cdot mL^{-1}$ DNAse (bovine pancreas, grade II; Sigma-Aldrich, St. Louis, MO, USA), 500 $\mu g \cdot mL^{-1}$ lysozyme (chicken egg white, grade VI; Sigma-Aldrich), 4 mM $MgCl_2$ (Sigma-Aldrich), and 5 mM imidazole (Sigma-Aldrich). The STxB expressing cells were lysed by sonication, while the STxB–eGFP expressing cells were lysed by liquid homogenization with the use of a French press (since, in this case, seem to avoid protein precipitation in inclusion bodies). The lysates were clarified by centrifugation at 20 000 ***g*** for 1 h, and the supernatants were applied to a Ni-NTA agarose resin (Qiagen, Hilden, Germany) pre-equilibrated with lysis buffer. The hexahistidine-tagged proteins were eluted from the Ni-NTA agarose resin using an elution buffer (200 mM imidazole in lysis buffer). For STxB, an additional purification step was performed *via* size exclusion chromatography (SEC) using a Superdex 75 Hiload 16/60 column (GE Healthcare, Chicago, IL, USA). The protein was eluted in PBS (pH 7.4) and incubated overnight with SUMO hydrolase (dtUD1), in order to cut the tag from the STxB–eGFP-SUMO fusion protein. STxB–eGFP was then purified *via* Ni-NTA affinity chromatography and SEC, using a Superdex 200 10/300 GL column (GE Healthcare) and PBS as carrier buffer. Both proteins were concentrated *via* ultrafiltration (cutoff 30 kDa, Amicon Ultra-15; Merck Milipore, Burlington, MA, USA). Aliquots of the proteins were then flash-frozen in liquid nitrogen and stored at −80 °C. The purity of the protein was estimated by SDS–PAGE and the concentration by NanoDrop ND-1000 Spectrophotometer (Marshall Scientific, Hampton, NH, USA). A stock sample of the STxB constructs was taken from −80 °C storage and thawed directly before analysis. The homogeneity of the samples of the STxB constructs was confirmed by dynamic light scattering analysis using Zetasizer Ultra (Malvern Panalytical, Malvern, UK).

STxB labeling

The His-tagged STxB protein was labeled with either fluorescein isothiocyanate (F3651; Merck Life Sciences, Darmstadt, Germany) or with the quencher ATTO540Q (AD 540Q-31; Atto-Tech, Amherst, NY, USA) *via* primary amines, that is, lysines. This was performed as previously described [25]. The labeled protein was then purified through a NAP-5 column (GE Healthcare) in PBS pH 7.4 for the removal of unbound fluorophore.

Differential scanning fluorimetry (nanoDSF)

The thermal stability of STxB and FITC-labeled STxB was determined by differential scanning fluorimetry monitoring intrinsic fluorescence (nanoDSF) using a Tycho NT6 instrument (Nanotemper Technologies, Munich, Germany). Two capillaries were filled with samples of unlabeled STxB (0.1 $mg \cdot mL^{-1}$ protein in PBS pH 7.4), and STxB amino coupled with FITC (0.1 $mg \cdot mL^{-1}$ protein in PBS pH 7.4). Intrinsic fluorescence was monitored at 330 and 350 nm (tryptophan and tyrosine emission wavelengths, respectively) during a thermal ramp. The inflection temperature (T_i) was calculated as the inflection point in the shift of intrinsic fluorescence. The same experiment was performed in duplicate with samples that were kept at 4 °C for a week after thawing.

Culture and seeding of cells

Ramos (ATCC® CRL-1596™), Daudi (ATCC® CCL-213™), and K562 cells (ATCC® CCL-243™) were cultured in RPMI-1640 (cat. no. F1215; Merck Sharp & Dohme Ltd., Hoddesdon, UK). The human HT-29 colon carcinoma cell line was cultured in McCoy's cell culture medium (cat. no. 16600082; Invitrogen, Carlsbad, CA, USA). Both types of cell culture media were supplemented with 10% fetal bovine serum (cat. no. F6765; Sigma-Aldrich; Merck KGaA, Darmstadt, Germany), 2 mM L-glutamine (cat. no. K0283; Merck Sharp & Dohme Ltd.), 100 IU penicillin, and 100 $\mu g \cdot mL^{-1}$ streptomycin (cat. no. A2213; Merck Sharp & Dohme Ltd.). For Daudi cells, 1% sodium pyruvate (Sigma-Aldrich) was also added.

For RT-CBA (see below) with Daudi, Ramos, and K562, the suspension cells were seeded and tethered on Petri dishes as described by Bondza *et al.* [26]. For easy comparison between the binding of STxB–FITC and STxB–eGFP to living cells, both ligands were measured simultaneously using LigandTracer MultiDish 2 × 2 (Cat. No. 1-4-201; Ridgeview Instruments AB, Uppsala, Sweden). MultiDish 2 × 2 was coated with Polydopamine for HT-29 cells since improvement of cell attachment was needed. In all measurements, a cell-free area of the compartment was used as a reference. Cell seeding to the MultiDish was performed according to the manufacturer's instructions.

Real-time cell-binding assays

The interactions of FITC-labeled STxB and STxB–eGFP with HT-29, Daudi, and Ramos cells were measured in a RT-CBA with LigandTracer® Green (Ridgeview Instruments AB), using a blue (488nm) − green (535 nm) detector. Measurements were conducted in cell culture medium (see above) and started with a short baseline measurement in the absence of labeled protein. STxB–FITC or STxB–eGFP was then added to the medium to give the specified final concentration. Association phase data were subsequently recorded for a defined time (typically 3–6 h). In some cases, more STxB was added to get data for multiple concentrations in series. The solution was then replaced with fresh medium to monitor the dissociation of STxB from the cells. Experiments at different temperatures were performed by placing the complete instrument in a temperature-controlled cabinet [27]. For understanding the impact of time on the binding mechanism of the STxB constructs, STxB–eGFP or STxB–FITC was added stepwise at shorter (0.5 + 1 h) or longer (3 + 3 h) incubation times. For the proximity assays, a defined concentration of STxB–eGFP or STxB–FITC was incubated until a clear signal increase was obtained followed by the addition of STxB labeled with the quencher molecule ATTO540Q. If the two STxB constructs bound in proximity on the cell surface, a decrease in the slope of the binding curve was expected. To exclude competition between the STxB constructs as a cause for signal decrease, control experiments with unlabeled STxB were performed.

Data analysis

RT-CBA traces produced with LigandTracer Green were analyzed using the evaluation software TRACEDRAWER 1.8 (Ridgeview Instruments AB). Data were normalized to allow a simple comparison of binding curves. In Figs 4 and 7, the signal was normalized by setting to 100% at the end of the second incubation phase for better comparison between different temperatures and incubation times. In Fig. 6, the signal was normalized after 3 h of STxB incubation to enable comparisons between the association and dissociation phases at different temperatures. For estimating the internalization rates from Fig. 8A, data from concentration series of STxB–eGFP (3–270 nM) were normalized at 30 min from the association phase. Percentage of internalized STxB–eGFP per hour relative to the number of surface-bound STxB–eGFP was obtained by relating the slope of the linear increase (from the time points from 2 to 3 h of incubation) to the surface-bound STxB–eGFP at equilibrium conditions (signal plateau) at lower concentrations (3 nM). For the proximity experiments (Fig. 9), to clearly visualize the quenching effect, data were normalized by setting the baseline levels to zero and the time point when it was either STxB-ATTO540Q or unlabeled STxB was added to 100%.

Detailed kinetic information for interactions can be estimated from binding curves in the form of association and dissociation rates, theoretically defined as kinetic parameters (k_a and k_d, respectively). For a Langmuir 1 : 1 binding model where a reversible interaction between two species occurs in one step ($L + T \leftrightarrow LT$), the binding function is given by

$$\frac{d[LT]}{dt} = k_a \times [L] \times [T] - k_d \times [LT].$$

In real-time techniques for measuring interactions, it is assumed that the number of targets ($[T]$) is constant over time and that depletion of the ligand (L) is negligible. If these assumptions are met, the measured signal (B) is proportional to the number of complexes (LT) formed. Thus, the equation above can be written as follows:

$$\frac{d[B]}{dt} = k_a \times [L] \times (B_{max} - B) - k_d \times B,$$

B_{max} represents the signal when receptors are saturated with ligand (L).

Confocal microscopy

HT-29 and Daudi cells were immobilized on nontreated μ-slides (80821; Ibidi, Martinsried, Germany) for immunofluorescence studies. Cells were incubated for 3 h with STxB–FITC and STxB–eGFP to a final concentration of 30 nM (Fig. 5) or 90 nM (Fig. 8D, STxB–eGFP). For cell membrane detection, cells were stained with the dye CellMask™ Deep Red Plasma Membrane Stain (C10046; Invitrogen) according to the manufacturer's protocols. Slides were captured with a Zeiss LSM 700 confocal microscope (Zeiss, Oberkochen, Germany). Images were processed using IMAGEJ software (U. S. National Institutes of Health, Bethesda, MD, USA).

Results

Analysis of thermal stability of STxB by nanoDSF

To evaluate how STxB was affected by FITC-labeling, a thermal shift analysis monitoring the intrinsic fluorescence at 330 and 350 nm from 35 °C to 95 °C was performed. The absorbance ratio was plotted as a derivative to get the inflection temperatures for the different measurements (Fig. 1). A 6.4 °C difference in the inflection temperature between unlabeled STxB and the labeled form STxB–FITC (78.7 °C and 72.3 °C, respectively) indicates that the stability of STxB is negatively reduced by the labeling, but a steep denaturation curve indicates that the protein is still folded. The same result was observed after storage for a week at 4 °C.

Evaluation of STxB-specific interactions with Gb3-positive cell lines

The ability of STxB to bind to cells and internalize while fused to the small molecule fluorescein or the protein eGFP was explored. Daudi, Ramos, and HT-29 cells were chosen since they have high levels of Gb3 on their surface. The K562 cell line was used as negative control as it does not contain extracellular Gb3.

First, STxB–FITC was used to confirm that STxB only interacts with Daudi cells with Gb3 on the extracellular surface (Fig. 2). After seeding and tethering cells onto a Petri dish, STxB–FITC was added to a final concentration of 30 nM and the association was monitored for almost five hours. This was followed by a dissociation rate measurement using fresh medium without STxB–FITC (the small shifts in signal at the start and end of the association phase are typical from real-time methods associated, in this case, with fluorescent liquid and not from actual interaction events).

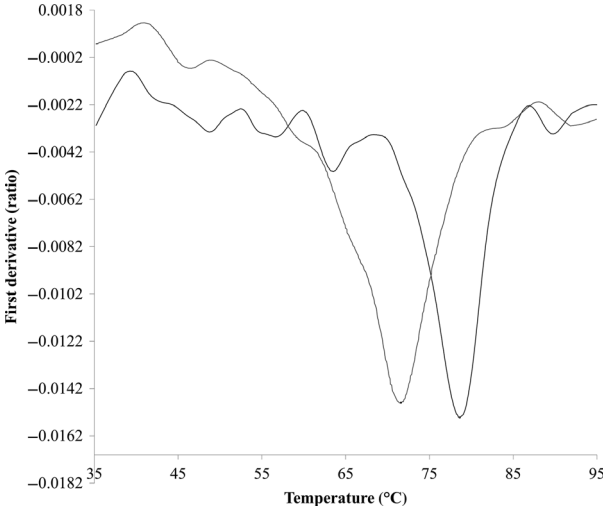

Fig. 1. nanoDSF analysis of STxB and STxB–FITC. First derivative of the ratio of the intrinsic fluorescence detected at 350 and 330 nm of STxB–FITC (gray) and STxB unlabeled (black) both at a final concentration of 0.1 mg·mL^{-1}, as a function of temperature.

STxB was found to interact reversibly with the cultured Daudi cells (Fig. 2, black), but not with K562 cells (Fig. 2, gray). Both the association and dissociation phases had an initial 'burst', followed by a linear phase, indicating that there are (at least) two events taking place, with a first rapid event being followed by a slower more continuous process. Control experiments with reactive uncoupled FITC or a fusion eGFP (fusion protein with the same GSGS linker strategy) were also conducted and did not show unspecific binding to target cells (data not shown).

Secondly, the interaction was confirmed with STxB–eGFP (90 nM) and HT-29 cells (Fig. 3) while prolonging the incubation time to obtain more information on the slower continuous process observed for STxB–FITC. The biphasic behavior was also observed for STxB–eGFP, with the linear phase being constant for more than 12 h.

The characteristics of STxB–FITC and STxB–eGFP interactions with Gb3 expressing cell lines were further explored. Two different concentrations and two incubation times were used in order to elucidate the mechanistic basis for the biphasic behavior seen during both the association and dissociation part of the measurement (Fig. 4).

When the STxB variants were incubated with Ramos cells for short times (0.5 + 1 h), only the initial nonlinear phase was seen during the association phase (Fig. 4A,B), similar to a simple 1 : 1 interaction with one reversible step. However, signs of a more

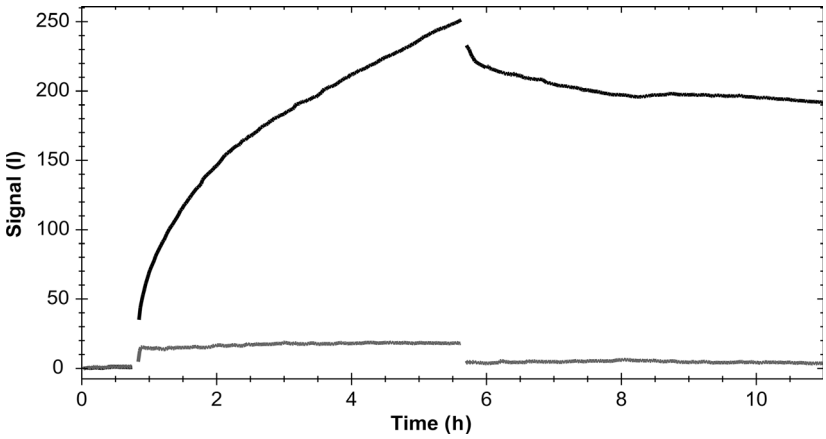

Fig. 2. Analysis of STxB–FITC interactions with Gb3-positive and Gb3-negative cells. RT-CBA traces for 30 nM STxB–FITC incubated with Daudi (black) and K562 (gray) cells at room temperature. Association was monitored for 5 h after baseline acquisition, and the dissociation rate was studied after replacing the medium with fresh medium without STxB–FITC (t = 5.6 h). The small shifts in signal at the start and end of the association phase are due to adding/removing a fluorescent compound and not actual interaction events.

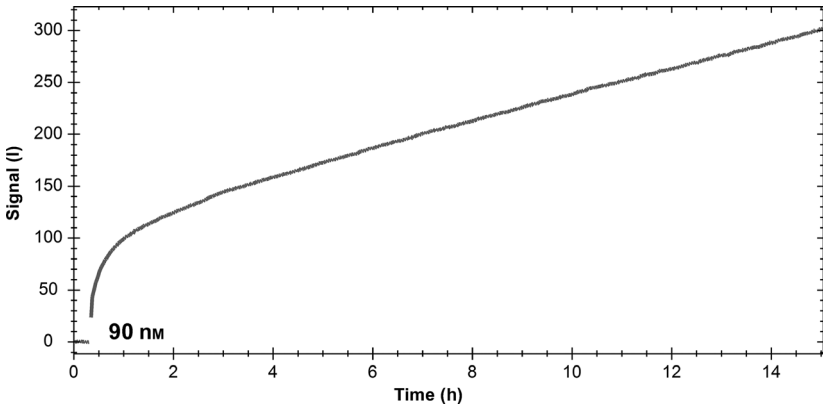

Fig. 3. Analysis of STxB–eGFP interactions with HT29 cells. RT-CBA traces of 90 nM of STxB–eGFP incubated for more than 12 h at room temperature.

complex interaction were observed in the dissociation phase, with an initial rapid and considerable release of labeled STxB, followed by a stable signal that did not show any tendency to return to baseline. In contrast, when the STxB variants were incubated for longer times (3 + 3 h), the association rate was biphasic, with an initial rapid signal increase, followed by a slower linear increase (Fig. 4C,D). Moreover, the initial rapid release of labeled protein in the dissociation was less pronounced when incubation times were longer. The same behavior was seen for both variants of STxB, but with differences in the kinetics and magnitude of the effects. The interaction data suggest that for both STxB variants, two processes occur: (a) a direct interaction between STxB and Gb3 receptors, and (b) an internalization of STxB. Furthermore, the amount of internalized STxB appears to depend on the incubation time. In addition to STxB internalization, yet another process involving production or recycling of Gb3 by metabolically active cells may increase the concentration of Gb3 on the surface if the time for the experiment is long relative to the rate of synthesis/recycling.

Confirming internalization of STxB

To investigate whether the STxB variants were in fact internalized, as suggested by the experiments above (Fig. 4), an orthogonal live-imaging confocal experiment was performed. STxB–eGFP and STxB–FITC were incubated with Daudi cells for 3 h, whereafter a Z stack from the confocal was imaged (Fig. 5). Both STxB variants were indeed internalized after 3 h, and signs of tubular membrane formations could be observed. It was also observed that STxB constructs were not evenly distributed on the cell membrane and a higher level of STxB appears to be in clusters on the cell surface and in tubular formations.

Effect of cell metabolism on STxB interactions with cells

To understand how the metabolic status of cells influences their interaction with STxB, RT-CBAs were performed at different temperatures (Fig. 6). A first series of experiments was performed on Daudi cells (Fig. 6A–C). When incubating with 30 nM STxB–

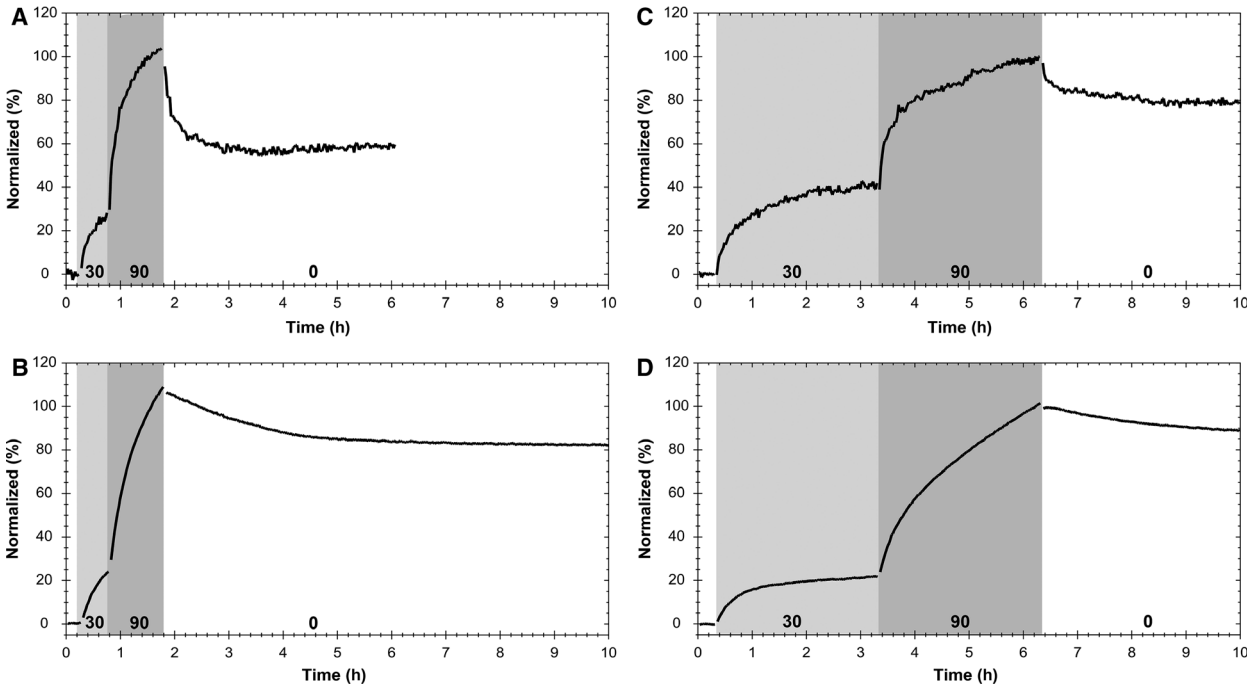

Fig. 4. Analysis of the effect of STxB–FITC and STxB–eGFP concentrations and incubation times on cell interactions. RT-CBA with 30 and 90 nM STxB–FITC (A, C) or STxB–eGFP (B, D) incubated with Ramos cells for either 0.5 + 1 h (A, B) or 3 + 3 h (C, D).

eGFP for 3 h at low temperature (8 °C), the interaction seemed to reach equilibrium (Fig. 6A, black). When fresh medium was added to follow dissociation, the decrease was linear. The measured interaction curve fitted a 1-step, 1 : 1 interaction model very well, with a resulting apparent affinity (K_D) of 1.92 nM (with $k_a = 2.6 \times 10^3$ $M^{-1}{\cdot}s^{-1}$ and $k_d = 5.1 \times 10^{-6}{\cdot}s^{-1}$). However, time turned out to be a crucial parameter for the kinetics of the STxB interaction. By increasing the incubation time to more than 3 h, a second phase with an almost linear signal increase was observed during the association (Fig. 6A, gray).

To explore the effect of cell metabolism on the kinetics and to determine whether the second phase of the rate is due to a biological event, the experiments were repeated at 37 °C (Fig. 6C). The initial signal burst in the association phase was faster and leveled off within just one hour, and the linear phase was more distinct and with a higher slope compared to the experiments at 8 °C.

The first part of the association curve is interpreted as the actual binding of STxB–eGFP to the cells, with a signal that increased rapidly until a pseudo/quasiequilibrium-binding level was reached, at a rate that increased with temperature (Fig. 6B,C). The subsequent continuous linear signal increase is not consistent with any process where receptors become saturated. This may be explained by internalization, supported by the observation that the dissociation at 37 °C showed a relatively rapid signal decrease during the first hour, followed by a stable signal that did not return to baseline. It would suggest that roughly 80% of the fluorescence remains within Daudi cells (Fig. 6C).

The interaction between STxB–eGFP and HT-29 cells showed a similar behavior as observed with Daudi cells (Fig. 6D–F). Again, at 8 °C, prolonging the incubation time for longer than 3 h showed that the interaction was not adequately described by a 1 : 1 binding process (Fig. 6D). However, when considering the data from the association and dissociation in Fig. 6D (black curve), a similar affinity value was obtained (K_D = 1.68 nM), but the binding and dissociation of STxB–eGFP with HT-29 cells was slightly faster compared to the same interaction on Daudi cells ($k_a = 1.11 \times 10^4$ $M^{-1}{\cdot}s^{-1}$ and $k_d = 1.87 \times 10^{-5}{\cdot}s^{-1}$). When the temperature was increased, a faster interaction was seen (Fig. 6E,F).

The effect of increasing the STxB concentration was also tested at different temperatures, in order to distinguish the binding signal from signal changes caused by secondary processes related to internalization or metabolic processes in the cell (Fig. 7). When STxB–FITC or STxB–eGFP was incubated at an

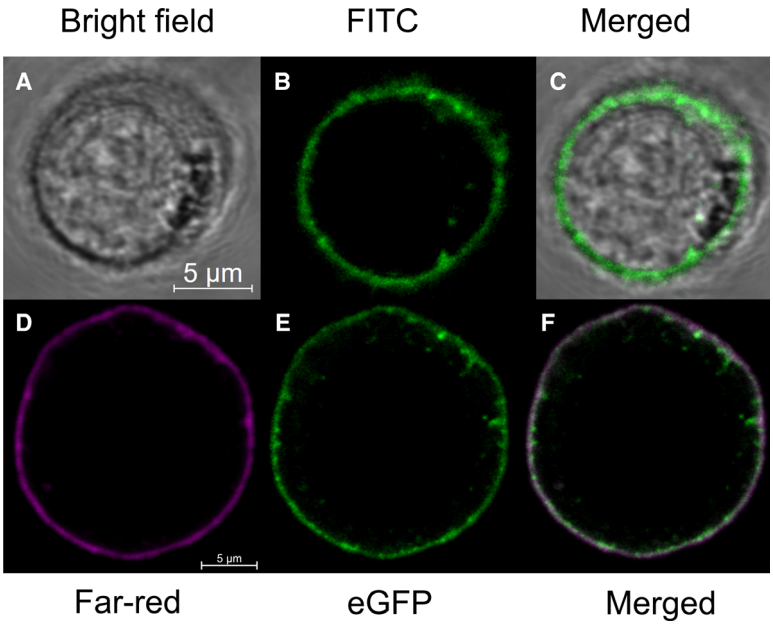

Fig. 5. Live imaging of Daudi cells incubated with STxB–FITC (A–C) and STxB–eGFP (D–F) for 3 h. (A) Transmitted light imaging on Daudi cells. (B) FITC fluorescence in the middle layer of the Z scan. (C) Overlap of the fluorescence and transmitted light images in A and B. (D) Far-red dye staining on the plasma membrane. (E) eGFP fluorescence in the middle layer of the Z scan. (F) Overlap of fluorescence images in D and E.

initial 30 nM concentration, the signal approached an equilibrium (disregarding the second linear phase that was evident in some cases). When a consecutive incubation at 90 nM was included, a second signal level was reached (Fig. 7). This increase was much higher than could be expected from a 1 : 1 binding model. It indicated that more receptors became accessible or available for STxB binding during the second incubation step with a higher concentration. The interaction of STxB–FITC and HT-29 cells appeared to have faster kinetics than STxB–eGFP also at 37 °C and 8 °C (Fig. 7). Moreover, data suggest that the level of dissociation of the STxB constructs is lower at 8 °C comparing with higher temperatures.

Analysis of STxB binding vs. internalization

To better understand the difference between the actual interaction between STxB and cells and the internalization of the toxin, the concentration dependency of the interaction was studied in more detail. HT-29 cells were incubated with a concentration series of STxB–eGFP. By normalizing the data at 30 min (first part of the 3 h association), it can be seen that the curve shape is similar for the different concentrations for the first half hour of incubation (Fig. 8A). At longer incubation times, it seems that an equilibrium binding level is reached within 1 h at a concentration of 3 nM. At higher concentrations, the signal increases linearly in a concentration-dependent fashion.

The internalization rate, relative to the amount of bound STxB at different concentrations (Fig. 8B), was estimated by relating the slope of the linear increase to the amount of surface-bound STxB–eGFP at equilibrium at 3 nM. It was observed by a confocal microscopy experiment that, when HT-29 cells are incubated 3 h with a final concentration of 90 nM, 40 ± 2% of the STxB–eGFP signal is at the intracellular environment (Fig. 8C). The intracellular rates obtained by the RT-CBAs at the same concentration show that 18% of the surface-bound STxB–eGFP is being internalized per hour, which reflects that approximately 2–2.5 h from the linear increase signal, 37% to 46% of the STxBeGFP is in the intracellular environment. The experiment shows that not only the amount of bound STxB increases but also that internalization of STxB–eGFP is promoted at higher concentrations, supporting a 2-step mechanism where binding is followed by internalization.

Analysis of STxB clustering on cell surfaces

The internalization of STxB is a complex process involving binding to Gb3 receptors, subsequent induction of cell membrane curvature and receptor clustering, and formation of tubular endocytic pits [7]. To better understand the data in Fig. 8 and explore if the increased concentration affects clustering of STxB upon binding to Gb3, experiments exploring the effects of adding more STxB on already bound labeled STxB were performed with cells. For the experiments,

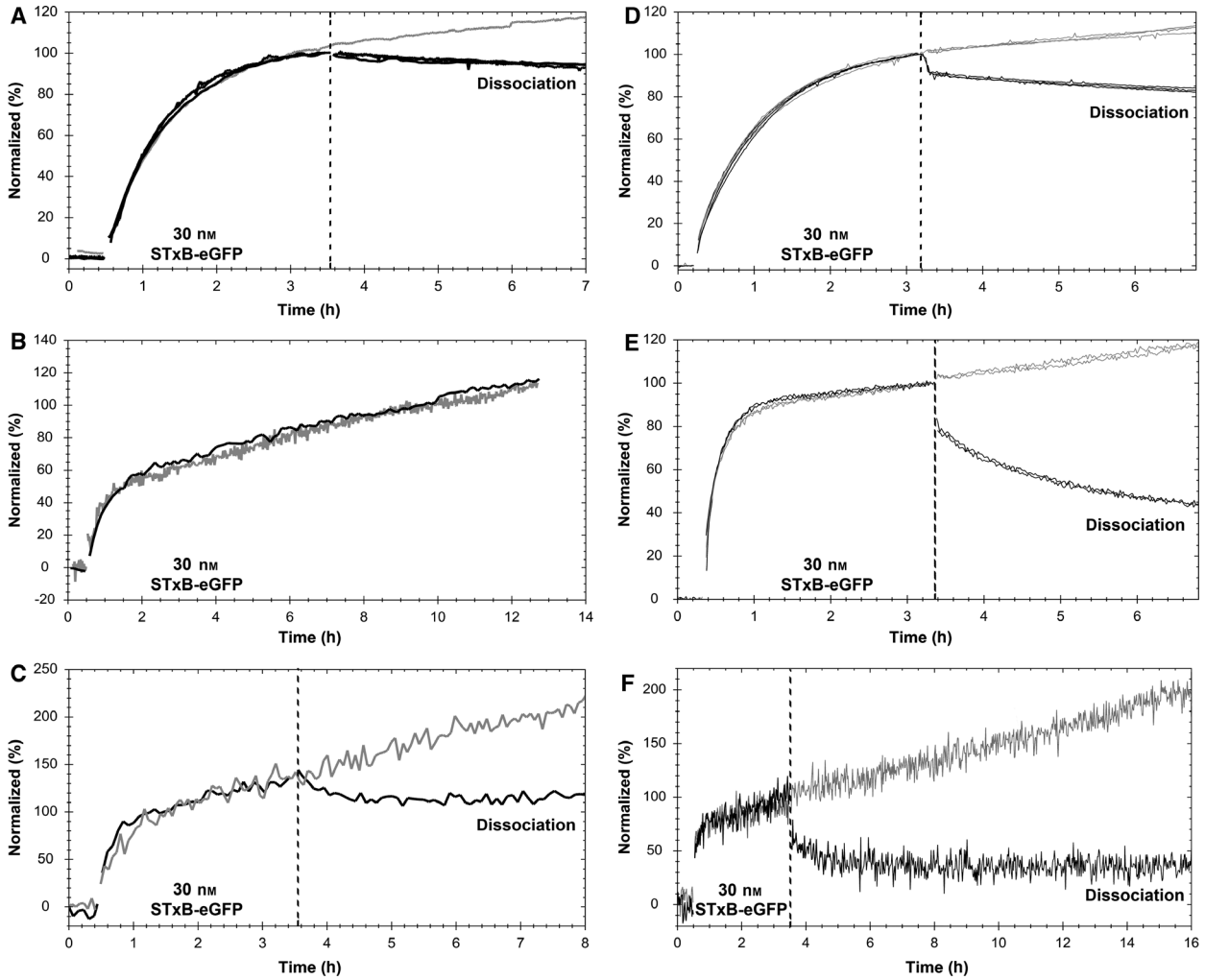

Fig. 6. Kinetic studies of interactions between STxB–eGFP and cells at different temperatures. RT-CBA with Daudi (A–C) and HT-29 cells (D–F) at 8 °C (A, D), room temperature (B, E) and 37 °C (C, F). Incubation for 3 h (black) and > 3 h (gray). The dotted line represented the time point where dissociation was performed.

unlabeled STxB and STxB labeled with a quencher (STxB-ATTO540Q) were used.

Quenching assays were performed by allowing STxB–FITC and STxB–eGFP to interact with Ramos cells for 1 or 4 h, respectively (Fig. 9A,B). This was followed by a subsequent addition of STxB-ATTO540Q (black trace, shaded area). Two reference experiments were performed. In the first experiment with STxB–FITC, a similar addition was done with unlabeled STxB (gray trace, shaded area; Fig. 9A) while with STxB–eGFP, nothing was added (gray trace, shaded area; Fig. 9B). The addition of STxB–ATTO540Q resulted in an immediate slight decrease in the fluorescent signal. Since the signal comes from bound STxB–FITC and STxB–eGFP, it confirms that the added STxB binds in proximity to the labeled STxB. As the signal decrease can be a consequence of physically displacing the fluorescent STxB constructs or quenching of their fluorescence, a second reference experiment was performed that consisted of the addition of unlabeled STxB to STxB–FITC. In this experiment, no signal reduction was observed, suggesting that there was no displacement of already bound FITC-labeled STxB (gray trace, shaded area; Fig. 9A).

To further explore whether the decreased signal upon addition of STxB-ATTO540Q was due to a displacement of STxB–eGFP on the cells, an actual displacement assay (without affecting the fluorescence with a quencher) was performed with unlabeled STxB and both Ramos and HT-29 cells (Fig. 9C,D). When unlabeled STxB was added to cells preincubated with STxB–eGFP, an unexpected increase in the signal was

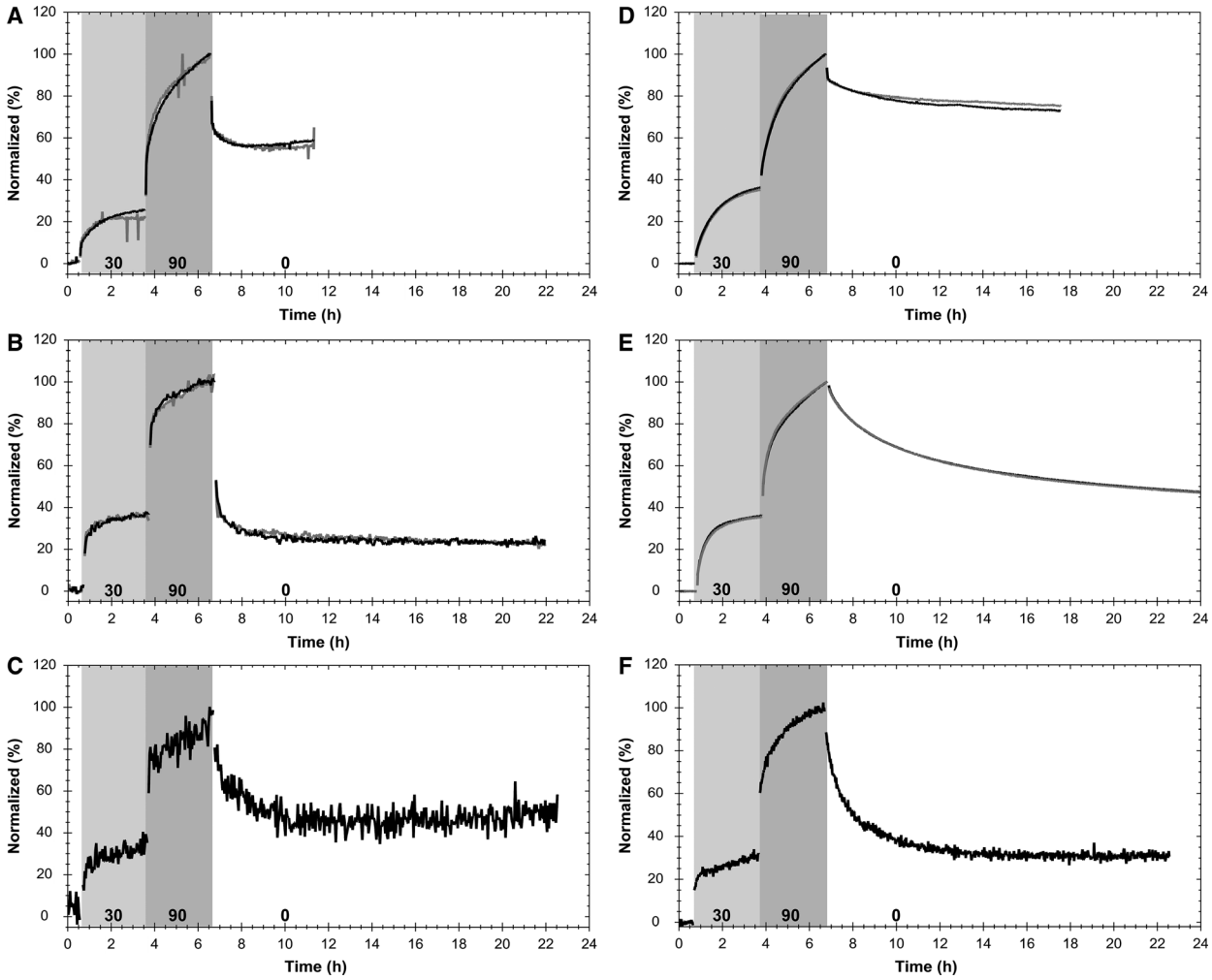

Fig. 7. Kinetic studies of interactions between STxB variants and HT-29 cells at two concentrations and different temperatures. RT-CBA experiments at 8 °C (A, D), room temperature (B, E) and 37 °C (C, F). STxB–FITC (A–C) and STxB–eGFP (D–F) were added in two consecutive steps to final concentrations of 30 and 90 nM, followed by dissociation.

observed (Fig. 9C,D). There was clearly no displacement of already bound STxB–eGFP. Instead, by adding unlabeled STxB, additional binding and/or internalization of STxB–eGFP was promoted. This could be related to the STxB binding induced clustering and subsequent internalization, which was more effective at higher STxB concentrations.

Discussion

In this paper, a time-resolved method for studying interactions with cells was used to show how Shiga toxin subunit B (STxB) binds to and internalizes into different cancer cell lines. In addition, by studying the effects of temperature, concentration, and time, new features of STxB function were revealed. STxB is of great pharmaceutical interest because it can potentially be exploited in the development of therapies with higher tumor specificity, thus reducing side effects and increasing efficacy. In the case of STxB, this could offer new therapeutic strategies for colon cancer or lymphoma. Internalizing toxins are considered to be promising delivery tools, since such toxins have naturally acquired specific characteristics through interaction with their hosts. The nontoxic B-subunit of the bacterial STxB, known for rapid binding and internalization, has been exploited as a delivery tool for specific compounds in tumor imaging or therapy, thus successfully demonstrating a useful functionality in preclinical models [28].

Although STxB has been reported to be easily engineered with functionality [29,30], the cellular mode of

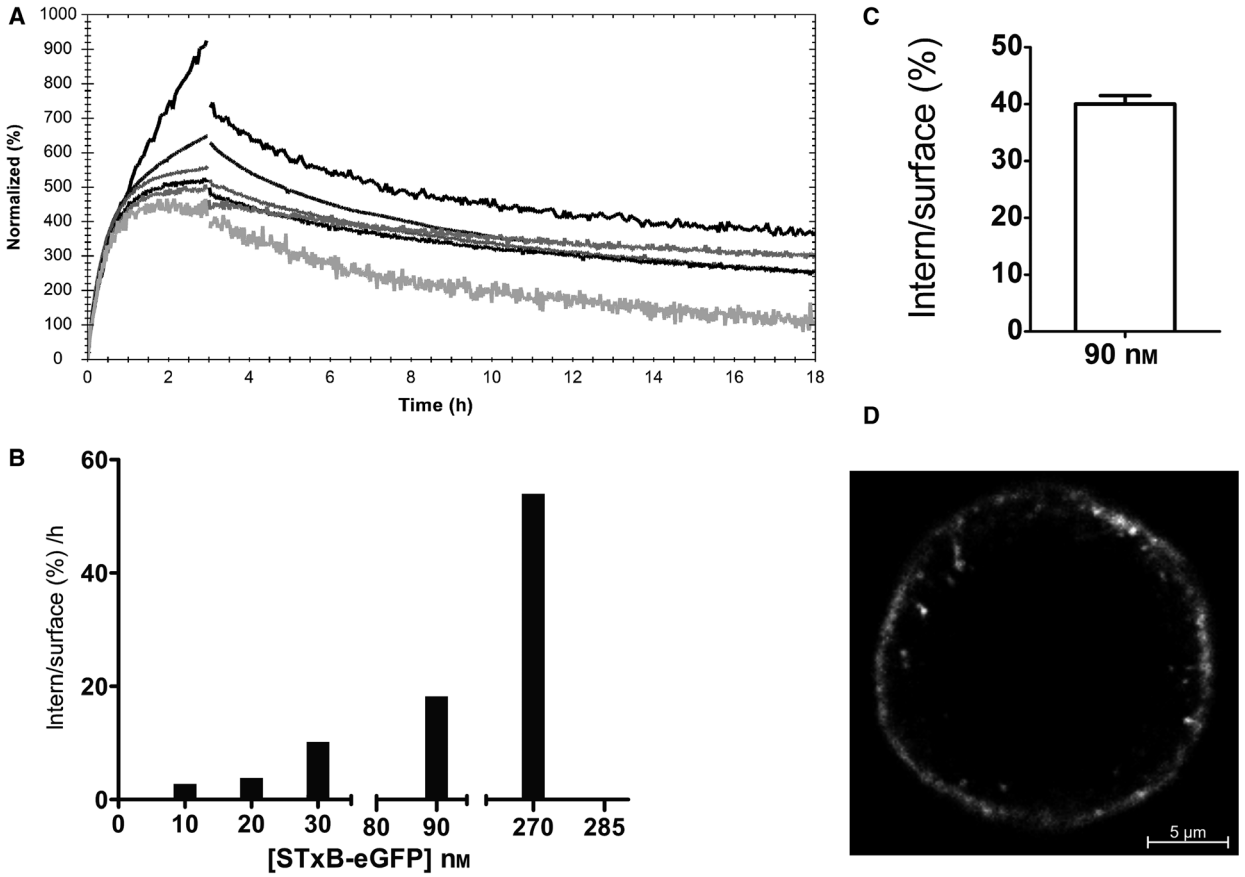

Fig. 8. Analysis of STxB–eGFP HT-29 cell interaction and internalization. RT-CBA experiments with concentration series of STxB–eGFP from 3 to 270 nM, normalized at 30 min (A). Percentage of internalized STxB–eGFP per hour relative to the number of surface-bound STxB–eGFP (B). The quantification of internalized STxB–eGFP, upon 3-h incubation with a final concentration of 90 nM, is represented as the intensity of fluorescence normalized to the area between the membrane binding and internalization of STxB–eGFP (C). Results represented in bars are expressed as the mean ± SD ($n = 3$). eGFP fluorescence in the middle layer of the Z scan in living HT-29 cells (D).

action is complex, involving not only binding to the receptor, but also receptor clustering, induction of membrane curvature and endocytosis. Bioengineering of STxB for specific applications, for example, involving conjugating or fusing it to specific peptides or compounds, requires access to novel technologies for evaluating and optimizing the efficacy and characteristics of the mechanistic and kinetic details of binding and uptake of new constructs. RT-CBA is a suitable, but, yet, largely unexplored, technique as it can detect fluorescent molecules or fluorescent proteins at the surface and intracellular level over time, and thus provide time-resolved information on how engineered STxB constructs localize in living cells.

The present study demonstrated that RT-CBA is indeed a very useful technique for studies of interactions with living cells. It revealed that STxB has the capacity to carry small molecules and small proteins such as eGFP into cells. Indeed, STxB was able to carry a molecule four times bigger than the monomer (STxB is 7.7 kDa and eGFP is 32.7 kDa) to an intracellular environment. There is an impressive capacity for the STxB pentamer to carry 5 eGFP proteins (each as STxB monomer fusion). As expected, the process appeared to be slower for STxB–eGFP than for the smaller STxB–FITC construct. A promising aspect is the selective and rapid uptake of STxB by HT-29, Ramos, and Daudi cells, which may reflect a high capacity of STxB to penetrate tissue. The data thus confirm that STxB demonstrates a high flexibility as a scaffold for engineering of novel therapeutics. Furthermore, the new methods developed gave crucial information about specific variables affecting the binding and internalization of different STxB constructs.

To better interpret the complexities seen in the data, we also need input from the field of cell membrane biophysics which can help our understanding of membrane mechanical processes caused by Shiga toxins.

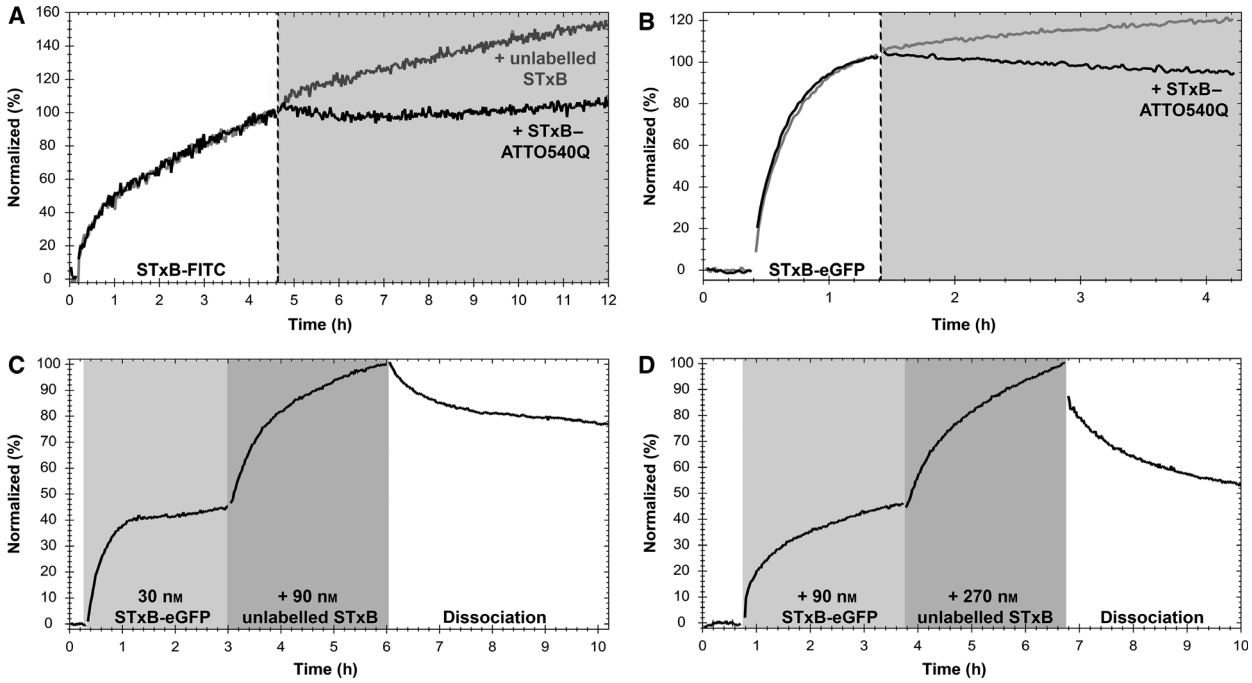

Fig. 9. Analysis of STxB clustering on cell surfaces. RT-CBA experiments. (A, B) Quenching assays on Ramos cells incubated with 30 nM STxB–FITC (A) and 90 nM STxB–eGFP (B) for 4 or 1 h, respectively. The shaded area represents a subsequent addition of 30 nM (A) or 270 nM (B) STxB–ATTO540Q (black trace, shaded area), 30 nM STxB (A, gray trace, shaded area) or nothing (B, gray trace, shaded area), the dotted line represented the time point where the addition was performed. (C, D) Displacement assays with 30 nM STxB–eGFP and Ramos cells (C) and 90 nM STxB–eGFP and HT29 cells (D) were incubated for 3 h. A subsequent addition of 90 nM (C) or 270 nM (D) of unlabeled STxB was followed by a 3-h incubation. The dissociation was monitored afterward.

An interesting temperature dependency of the STxB binding to living cells was observed. The STxB constructs dissociated less at 8 °C comparing with higher temperatures. This temperature-dependent effect on the binding of STxB was also observed in other studies with the shiga and cholera toxin [20]. A possible explanation could be due to the slower traffic of STxB [31], as well the more stable tubular formation overtime, which can lead to the STxB tubular entrapment [32]. On the other hand, when the interaction is evaluated at temperatures representing normal biological systems (37 °C), where metabolism, internalization, and degradation of ligands takes place, all of these may contribute to measurable effects. Under such conditions, also *de novo* synthesis or recycling of the receptors can change target availability, which can be reflected by signals that are not necessarily proportional to the number of ligand-target complexes on the cell surface. When combining data from two consecutive injections in the RT-CBA measurements, it is evident that the binding dynamics of STxB with cellular receptors is complex and cannot be characterized by a single 1-step interaction with a 1 : 1 stoichiometry. This is clearly a consequence of the far more complicated process of binding and internalization of the toxin in a biological evaluation context than a regular monovalent interaction. In addition, it is strongly dependent on temperature, concentration, and time. The apparent affinity is therefore not represented in a meaningful way by a simple dissociation equilibrium constant (K_D value), as often presented in the literature [15,16,24].

The interesting complex interaction from STxB may have several explanations of which one is the rapid endosomal recycling of Gb3 receptors, induced by Shiga toxin [31,33]. Some studies have shown that creating different STxB fusions do not change the capacity of the protein to internalize by tubular pits [34,35]. The biphasic binding curves, with an initial fast binding event followed by a slow linear increase, were observed. Since equilibrium binding was not reached, it could possibly involve a receptor recycling mechanism. The contribution of the two phases to the signal and the observation of a pseudoequilibrium at the end of the first phase were affected by the STxB concentration. Clearly, the more STxB bound to the cells (i.e., to the Gb3 receptors), the more efficient internalization. Increasing the temperature also enhanced the internalization process. A possible explanation might

be found in the mechanism of how STxB internalizes. STxB is known to generate the formation of tubular membrane invagination that guides the toxin into the cell [22]. Therefore, the linear increase observed might occur sooner with higher temperatures and high concentrations because STxB binds more rapidly and quicker reaches levels required to form tubular membrane. Hence, STxB cluster and tubular membrane promote more STxB to bind through the recruitment of receptors [21,36], as inferred from the linear increase in signals and a high amount of STxB–eGFP and STxB–FITC detected in the intracellular environment after 3 h by confocal microscopy. The conventional 1 : 1 model based on a constant number of targets over time is not accurate for such biological events in living cells. Other models than the 'one-to-one' are needed to estimate or compensate for all these biological differences, and conventional affinity values (assuming one-to-one) may be directly misleading. This means that there is plenty of evidence both from the past and in this paper that justifies the interaction deviating from the conventional 1 : 1 model.

Binding and internalization differences between cells types can be explained by the three Gb3-binding sites in each subunit B monomer, allowing for a tighter binding to the target cell. However, the STxB binding to cells might differ for different Gb3 species [28]. Pellizzari *et al*. [37] showed that the affinity of Shiga toxins is affected by the exact nature of the Gb3 fatty acid. In fact, the tightest binding was observed for mixtures of Gb3 species. It was shown that the fatty acyl chain of Gb3 strongly affects the lateral organization of STxB and impacts the overall membrane organization in phase-separated mixtures. The authors concluded that the protein cluster formation depends on the structure of the Gb3 fatty acid chains and area demand of unsaturated fatty acids, which in combination affect membrane bending [7,17]. We have previously seen differences in binding of the same ligand to the same target in various cells [37]. Moreover, the proximity assay between STxB labeled with fluorescent and quencher dyes also suggests that STxB proteins bind close to each other and accumulate in membrane clusters, increasing membrane tension and internalization.

Another interesting fact was the displacement studies of STxB–eGFP with unlabeled STxB. It was possible to observe that when unlabeled STxB was added in the presence of STxB–eGFP, a significant signal increase was observed. This can be explained by the equilibrium disturbance, where additional free ligands disturb the equilibrium state and promote more ligand binding to the free target, until eventually finding a new equilibrium state. As seen in Fig. 8, the equilibrium state at higher concentrations is apparently a state in which the relative internalization is more efficient. It was also possible to observe signs of tubular formations, that are characteristic for STxB, for STxB–eGFP with confocal microscopy. In addition, the amino coupling of the STxB with the fluorophore FITC still did not affect the internalization of the protein. An interesting side effect of nonlabeled STxB enhancing the function of labeled STxB is that the production of new conjugate STxB proteins might not need to produce perfectly pure conjugates, since nonlabeled moieties only potentiate the function. Considering the rapid internalization of the STxB constructs, it should be feasible to explore additional constructs to deliver different molecules or to target organelles at an intracellular level. In this case, measuring these kinds of interactions on living cells turned out to be crucial to characterize the possible new constructs with adequate data that can aid optimization and decision making.

In this study, we have shown that STxB has an impressive capacity to deliver cargo to the intracellular domain. The mechanism of action is complex, where the binding kinetics of STxB to cell membranes have been underestimated in different studies by not allowing enough time to detect secondary events, specially at lower temperatures. With better tools for characterization of the STxB internalization mechanisms, such as the RT-CBA approach discussed in this report, the full potential of the STxB capacity to deliver therapeutic agents to specific cells can be better understood, putatively leading to treatment modalities.

Acknowledgements

Microscopic imaging was performed with equipment maintained by the BioVis Platform at Uppsala University. We thank to Dr Arie Geerlof and Dr André Mourão (Institute of Structural Biology, Helmholtz Zentrum München) for providing help on protein expression and purification of the STxB constructs. This project has received funding from the European Union's Framework Programme for Research and Innovation Horizon 2020 (2014–2020) under the Marie Sklodowska-Curie Grant Agreement No. 675555, Accelerated Early staGe drug discovery (AEGIS).

Conflict of interest

Ridgeview Instruments AB (RIAB) develops and sells the device LigandTracer, which is described in the manuscript. João Encarnação, Jos Buijs, Karl

Andersson, and Hanna Björkelund are employed by RIAB. Jos Buijs, Karl Andersson, and Hanna Björkelund are shareholders of RIAB. RIAB acknowledges the adherence to all FEBS letter policies on sharing data and materials. All equipment described in the report is commercially available, and no patents restrict the use of the described assays. Valeria Napolitano, Giulia Opassi, Helena Danielson, Grzegorz Dubin, Grzegorz Popowicz, and Hélène Munier-Lehmann declare that they have nothing to disclose.

Author contributions

JCE, VN, GO, JB, KA, and HB designed all the experiments. JCE, VN, and GO performed all the experiments. JCE, VN, and GO wrote the manuscript. GMP designed the expression plasmids. GD, UHD, and HM-L provided crucial input and review on methodology. All authors discussed the results and commented on the manuscript.

References

1 Bae YH and Park K (2011) Targeted drug delivery to tumors: myths, reality and possibility. *J Control Release* **153**, 198–205.

2 Yao S, Zhu Y and Chen L (2013) Advances in targeting cell surface signalling molecules for immune modulation. *Nat Rev Drug Discov* **12**, 130–146.

3 Nasiri H, Valedkarimi Z, Aghebati-maleki L and Majidi J (2018) Antibody-drug conjugates: promising and efficient tools for targeted cancer therapy. *J Cell Physiol* **233**, 6441–6457.

4 Garcia-Alonso S, Ocana A and Pandiella A (2018) Resistance to antibody-drug conjugates. *Cancer Res* **78**, 2159–2166.

5 Sandvig K, Torgersen ML, Engedal N, Skotland T and Iversen T (2010) Protein toxins from plants and bacteria: probes for intracellular transport and tools in medicine. *FEBS Lett* **584**, 2626–2634.

6 Distler U, Souady J, Hülsewig M and Drmić-Hofman I (2009) Shiga toxin receptor Gb3Cer/CD77: Tumor-association and promising therapeutic target in pancreas and colon cancer. *PLoS ONE* **4**(8), e6813. http://dx.doi.org/10.1371/journal.pone.0006813

7 Watkins EB, Majewski J, Chi EY, Gao H, Florent J and Johannes L (2019) Shiga toxin induces lipid compression: a mechanism for generating membrane curvature. *Nano Lett* **19**, 7365–7369.

8 Mckenzie JE, Raisley B, Zhou X, Naslavsky N, Taguchi T and Sheff D (2012) Retromer guides STxB and CD8-M6PR from early to recycling endosomes, EHD1 guides STxB from recycling endosome to Golgi. *Traffic* **13**, 1140–1159.

9 Mckenzie JE (2009) The Recycling Endosome is Required for Transport of Retrograde Toxins. University of Iowa, Iowa City, IA.

10 Renard H, Garcia-castillo MD, Chambon V, Lamaze C and Johannes L (2015) Shiga toxin stimulates clathrin-independent endocytosis of the VAMP2, VAMP3 and VAMP8 SNARE proteins. *J Cell Sci* **128**, 2891–2902.

11 Batisse C, Dransart E, Brulle L, Bai S, Godefroy S and Johannes L (2015) A new delivery system for auristatin in STxB-drug conjugate therapy. *Eur J Med Chem* **95**, 483–491.

12 Barta P, Björkelund H and Andersson K (2011) Circumventing the requirement of binding saturation for receptor quantification using interaction kinetic extrapolation. *Nucl Med Biol* **32**, 3–7.

13 Geyer PE, Maak M, Nitsche U, Perl M, Novotny A, Slotta-Huspenina J, Dransart E, Holtorf A, Johannes L and Janssen K-P (2016) Gastric adenocarcinomas express the glycosphingolipid Gb3/CD77: targeting of gastric cancer cells with Shiga toxin B-subunit. *Mol Cancer Ther* **15**, 1008–1017.

14 Kostova V, Dransart E, Azoulay M, Brulle L, Bai S, Florent J-C, Johannes L and Schmidt F (2015) Targeted Shiga toxin-drug conjugates prepared via Cu-free click chemistry. *Bioorg Med Chem* **23**, 7150–7157.

15 Gallegos KM, Conrady DG, Karve SS, Gunasekera TS, Herr AB and Weiss AA (2012) Shiga toxin binding to glycolipids and glycans. *PLoS One* **7**, e30368.

16 Nakajima H, Kiyokawa N, Katagiri YU, Taguchi T, Suzuki T, Sekino T, Mimori K, Ebata T, Saito M, Nakao H *et al.* (2001) Kinetic analysis of binding between Shiga toxin and receptor glycolipid Gb3Cer by surface plasmon resonance. *J Biol Chem* **276**, 42915–42922.

17 Schütte OM, Werz DB, Patalag LJ, Weber LMC, Ries A, Ro W *et al.* (2015) 2-Hydroxy fatty acid enantiomers of Gb3 impact Shiga toxin binding and membrane organization. *Biophys Lett* **108**, 2775–2778.

18 Haller B, Staufer O, Dreher Y, Mersdorf U, Platzman I and Spatz JP (2019) One-pot assembly of complex giant unilamellar vesicle-based synthetic cells. *ACS Synth Biol* **8**, 937–947.

19 Falguie T, Baron C, Hanau D, Lingwood C, Goud B, Salamero J and Johannes L (2001) Targeting of Shiga toxin B-subunit to retrograde transport route in association with detergent-resistant membranes. *Mol Biol Cell* **12**, 2453–2468.

20 Fuchs G, Mobassaleh M, Donohue-Rolfe A, Montgomery RK, Grand RJ and Keusch GT (1986) Pathogenesis of shigella diarrhea: rabbit intestinal cell microvillus membrane binding site for shigella toxin. *Infect Immun* **53**, 372–377.

21 Aigal S, Claudinon J and Römer W (2015) Plasma membrane reorganization: a glycolipid gateway for microbes. *Biochim Biophys Acta* **1853**, 858–871.

22 Berland L, Gaus K, Windschiegl B, Aly MRE, Fraisier V, Florent J *et al*. (2007) Shiga toxin induces tubular membrane invaginations for its uptake into cells. *Nature* **450**, 670–675.
23 Björkelund H, Gedda L and Andersson K (2011) Comparing the epidermal growth factor interaction with four different cell lines: intriguing effects imply strong dependency of cellular context. *PLoS One* **6**, 1–7.
24 Poirier C, Van ED, Delord B, Johannes L and Roux D (2008) Specific adsorption of functionalized colloids at the surface of living cells: a quantitative kinetic analysis of the receptor-mediated binding. *Biochim Biophys Acta* **1778**, 2450–2457.
25 Stenberg J, Spiegelberg D, Karlsson H and Nestor M (2014) Choice of labeling and cell line influences interactions between the Fab fragment AbD15179 and its target antigen CD44v6. *Nucl Med Biol* **41**, 140–147.
26 Bondza S, Foy E, Brooks J, Andersson K, Robinson J, Richaletm P and Buijs J (2017) Real-time characterization of antibody binding to receptors on living immune cells. *Front Immunol* **8**, 1–11.
27 Encarnação JC, Barta P, Fornstedt T and Andersson K (2017) Impact of assay temperature on antibody binding characteristics in living cells: a case study. *Biomed Rep* **7**, 400–406.
28 Johannes L and Römer W (2010) Shiga toxins – from cell biology to biomedical applications. *Nat Rev Microbiol* **8**, 105–116.
29 Watanabe-takahashi M, Sato T, Dohi T, Noguchi N, Kano F, Murata M, Hamabata T, Natori Y and Nishikawa K (2010) An orally applicable Shiga toxin neutralizer functions in the intestine to inhibit the intracellular transport of the toxin. *Infect Immun* **78**, 177–183.
30 McKenzie J, Johannes L, Taguchi T and Sheff D (2009) Passage through the Golgi is necessary for Shiga toxin B subunit to reach the endoplasmic reticulum. *FEBS J* **276**, 1581–1595.
31 Martínez-Alonso E, Ballesta J and Martínez-Menárguez JA (2007) Low-temperature-induced Golgi tubules are transient membranes enriched in molecules regulating intra-Golgi transport. *Traffic* **8**, 359–368.
32 Müller SK, Wilhelm I, Schubert T, Zittlau K, Imberty A, Madl J, Eierhoff T, Thuenauer R and Römer W (2017) Gb3-binding lectins as potential carriers for transcellular drug delivery. *Expert Opin Drug Deliv* **14**, 141–153.
33 Ryou J-H, Sohn Y-K, Hwang D-E, Park W-Y, Kim N, Heo W-D, Kim M-Y and Kim H-S (2016) Engineering of bacterial exotoxins for highly efficient and receptor-specific intracellular delivery of diverse cargos. *Biotechnol Bioeng* **113**, 1639–1646.
34 Amessou M, Carrez D, Patin D, Sarr M, Grierson DS, Croisy A, Tedesco AC, Maillard P and Johannes L (2008) Retrograde delivery of photosensitizer (TPPp-O-β-GluOH)3 selectively potentiates its photodynamic activity. *Bioconjug Chem* **19**, 532–538.
35 Schubert T and Römer W (2015) How synthetic membrane systems contribute to the understanding of lipid-driven endocytosis. *Biochim Biophys Acta* **1853**, 2992–3005.
36 Pellizzari A, Pang H and Lingwood CA (1992) Binding of verocytotoxin 1 to its receptor is influenced by differences in receptor fatty acid content. *Biochemistry* **31**, 1363–1370.
37 Varasteh Z and Orlova A (2015) Comparing the measured affinity of 111In-labeled ligands for cellular receptors by monitoring gamma, beta, or X-ray radiation with three different LigandTracer® devices. *J Radioanal Nucl Chem* **304**, 823–828.